Diffusionlike motion of the modulation wave in incommensurate solids studied by NMR and NQR in a sinusoidal-electric-field gradient

G. Papavassiliou, M. Fardis, A. Leventis, and F. Milia
National Center for Scientific Research ''DEMOKRITOS,'' Ag. Paraskevi, Attiki, 153 10 Athens, Greece

J. Dolinšek, T. Apih, and M. U. Mikac
Jozef Stefan Institute, University of Ljubljana, Jamova 39, SLO-61111 Ljubljana, Slovenia
(Received 2 May 1996)

Slow random-walk-type motion of the modulation wave in structurally incommensurate systems represents a collective atomic self-diffusion in solids. The diffusion constant D for the thermally induced modulation wave motion has been determined using a technique based on NMR and nuclear quadrupole resonance (NQR) in an inhomogeneous electric-field gradient which varies sinusoidally with space. This technique is generally applicable to solids with a modulated superstructure. It is capable of measuring extremely low D values such as 10^{-15} cm^2/s, so that spatial motion is observed on a nanometric scale. The diffusive motion is discussed analytically on a scale small compared to the wavelength of the modulation wave, whereas large-scale diffusion is treated numerically. For small-scale motion, spin-echo decay curves in a NMR/NQR experiment show an exponential decay with the exponent proportional to the cube of time and the decay strongly varies over the incommensurate spectrum. For large-scale motion, the spin-echo decay is less strong and the variation over the spectrum vanishes. The diffusion constant has been determined experimentally in Rb_2ZnCl_4 by ^{35}Cl NQR and in K_2SeO_4 by ^{39}K NMR. In both cases, D behaves critically in the vicinity of the para-to-incommensurate transition and rapidly decreases on going deeper into the incommensurate phase. This can be explained by the mechanism of thermally induced depinning of the modulation wave at the impurity pinning centers. [S0163-1829(97)00117-3]

I. INTRODUCTION

Slow collective self-diffusion of atomic ensembles in solids with modulated structures has recently become a subject of intense research. Examples are the modulation wave motion in structurally incommensurate[1–4] (INC) and charge-density-wave (CDW) systems[5] and the superlattice motion in quantum flux lattices. These systems are characterized by the existence of a superstructure, the periodicity of which is generally incommensurately related to that of the underlying lattice; i.e., one periodicity is not a multiple of the other.

The dynamics of the superstructures is one of the open questions in condensed matter physics. Elementary excitations of the frozen-in modulation wave in structurally INC and CDW systems are harmonic oscillations[6] of the amplitude (amplitudon mode) and phase (phason mode) around the time-average values. Whereas the amplitude fluctuations are always small—except in the close vicinity of the para-INC transition temperature T_I—the phase fluctuations can be quite large. The theory of an ideal defect-free INC phase predicts the existence of a low-frequency translational phason mode (Goldstone mode), which moves frictionless throughout the crystal and induces transport phenomena such as superfluidity and superconductivity. These phenomena were in reality not observed in INC systems as the discrete lattice effects and impurities in real structures pin the modulation wave and restrict its translational degrees of freedom. The random spatial distribution of pinning centers and random pinning strength destroy the harmonic character of the thermally induced motion of the free modulation wave. The wave can overcome the pinning potential and stay locally depinned for a certain time by borrowing the thermal energy from the lattice, whereas it becomes pinned again after the energy is emitted back. Since thermal depinning is a random stochastic process, the resulting modulation wave motion is of a random-diffusion-like character. Similar depinning effects can be produced also by external forces like an ac electric field in CDW systems.

Thermal fluctuations of the modulation wave in the close vicinity of T_I have been reported recently in the INC phases of Rb_2ZnCl_4 (Refs. 1 and 2) and K_2SeO_4 (Ref. 2) in NMR line shape and spin lattice relaxation studies. Here we present evidence that the thermally induced modulation wave motion in INC systems is of a diffusional character. The diffusion coefficient D for the collective self-diffusion motion has been determined in a broad temperature interval. The values of D were found to be many orders of magnitude smaller from those characteristic for liquids. The smallness of these coefficients indicates that the effective diffusing particles have a large effective mass and can be associated with the ensembles of atoms lying on the modulation wave between pinning centers.

We present a method for the determination of extremely low diffusion coefficients which is based on the high-field NMR and zero-field nuclear quadrupole resonance (NQR) techniques in a spatially inhomogeneous electric-field gradient (EFG). The spatially inhomogeneous EFG is an intrinsic feature of a solid system without a perfect translational periodicity. It is produced by the displacements of electrically charged ions from their positions in a perfect lattice as a result of the presence of impurities or the existence of a modulated superstructure. The necessary condition for the

diffusion coefficient determination is a known spatial variation of the intrinsic inhomogeneous EFG, the situation which is found in modulated structures only. The use of the intrinsic EFG makes the method easily applicable in practice. The method is capable of measuring coefficients D as small as 10^{-16} cm^2/s and is under the above conditions superior to the standard method of high-field NMR in a linear magnetic-field gradient. A short account of a part of the theory presented here has been published in a recent Letter.[3]

II. DIFFUSION IN A SPATIALLY INHOMOGENEOUS ELECTRIC-FIELD GRADIENT

The standard method for the observation of diffusional effects in liquids and solids is the high-field NMR technique in the presence of a spatial magnetic-field gradient. The decay of the transverse magnetization is measured in the presence of a steady[7] or pulse[8] gradient. In case of a steady gradient, the spin-echo attenuation at time 2τ (τ is the spacing between the rf pulses in a two-pulse experiment) is given by

$$\frac{M(2\tau)}{M_0}=\exp\left\{-\frac{2\tau}{T_2}\right\}\exp\left\{-D\left(\gamma\frac{\partial H}{\partial z}\right)^2\frac{2\tau^3}{3}\right\}. \quad (1)$$

Here T_2 represents the transverse (spin-spin) relaxation time, γ the gyromagnetic ratio, and $\partial H/\partial z$ the linear magnetic-field gradient, assumed to have cylindrical symmetry around the z axis. The diffusion-induced damping is exponential with the exponent proportional to the cube of time.

The basic idea of detecting diffusional motions uses the fact that the nuclear resonance frequency varies in space in a controlled way; i.e., there exists a well-defined frequency-space relation. In case of a linear magnetic-field gradient, this relation takes a linear form

$$\omega(z)=\omega_0+\left(\gamma\frac{\partial H}{\partial z}\right)z \quad (2)$$

and every point in space along the z axis has a uniquely defined resonance frequency. The motion of molecules in space is observed via the changes of their resonance frequencies during the time of experiment.

The frequency-space relation in the above case is a consequence of a magnetic coupling between the nuclear magnetic dipole moments and the space-varying magnetic field. An analogous frequency-space relation can be obtained from the electrostatic coupling of nuclear electric quadrupole moments of nuclei with spins $I>1/2$ to the spatially varying electric-field gradients. If the EFG variation in space is known, one can determine the frequency-space relation for the quadrupole-perturbed Zeeman frequency (in high-field NMR) or pure quadrupole frequency (in zero-field NQR). The diffusional motion can be than observed in a similar way as in the magnetic case by measuring the quadrupole echo decay as a function of time. Here it is worth mentioning that the diffusion constant determination in a spatially varying EFG is possible also in the zero-field NQR technique and not only in the high-field NMR, as in the case of a spatially varying magnetic field.

In solids the frequency-space relation originates from the electrostatic interaction between the nuclei and the neighboring ions and is thus an intrinsic feature of a solid system. The necessary condition for the diffusion constant determination is a known spatial variation of the intrinsic EFG. Such a situation is generally seldom found. In perfect lattices the EFG repeats exactly at each physically equivalent site in the periodic unit cells and does not depend on space. Impurities destroy locally the translational periodicity and impose a spatial variation on the EFG. Due to the random spatial distribution of impurities, the variation of the EFG is also spatially random and a defined relation between space and resonance frequency cannot be derived. The same situation is encountered in solids with a glassy type of disorder.

There exists, however, a class of solids in which a well-defined frequency-space relation exists. These are the systems with a modulated structure like structurally INC systems. There, some local atomic property (e.g., atomic positions in the unit cell) is modulated in space in a sinusoidal manner and forms the modulation wave, the wavelength of which is usually large compared to the high-temperature unit cell length. A one-dimensional wave of atomic displacements can be described in the continuum approximation by a displacement field[9] u:

$$u(x,t)=A(t)\cos\varphi(x,t). \quad (3)$$

The wave is characterized by the amplitude A and the phase φ, which in the plane wave regime[9] varies in the direction x of the wave propagation as $\varphi=qx$. Here q is the wave vector of the modulation wave. Both A and φ undergo thermal fluctuations in time t.

The EFG tensor at a given lattice site reflects the distribution of surrounding ionic and electronic electric charges. In the modulated phase the atomic displacements from the paraelectric positions affect the EFG tensor elements V_{ij} and change their paraphase values. The changes are, however, small, and each element can be expanded in powers of the displacements u. In the local approximation,[9] V_{ij} depends on the displacement $u(x)$ at the position x only. This approximation is valid in the long-wavelength limit where the contribution to the EFG at a particular lattice site is coming from charges in a region of dimension small compared to the distance where the modulation displacement $u(x)$ changes appreciably. In that case we can write

$$V_{ij}(x)=V_{ij}^0+\left(\frac{\partial V_{ij}}{\partial u}\right)u+\frac{1}{2}\left(\frac{\partial^2 V_{ij}}{\partial u^2}\right)u^2+\cdots, \quad (4)$$

where V_{ij}^0 is the paraphase value. The quadrupole-perturbed NMR and pure quadrupole NQR frequencies can be written as a linear combination of the EFG tensor elements. Using Eqs. (3) and (4), we can write the resonance frequency in the form[9]

$$\omega(x)=\omega_0+\omega_1\cos(qx)+\omega_2\cos^2(qx)+\omega_3\cos^3(qx)+\cdots. \quad (5)$$

This equation represents a frequency-space relation in modulated structures and is basic for the observation of diffusional motions in a spatially inhomogeneous EFG. In contrast to the linear magnetic-field gradients, the space labeling is here not unique due to the periodicity of $\omega(x)$. Since the displacements u are small, the series of Eq. (5) converges rapidly and the leading behavior is given by the lowest-order terms. Un-

less forbidden by symmetry, this is the linear term. The case where the odd powers of $\cos(qx)$ are forbidden is found, e.g., in pure NQR of the A_2BX_4 family crystals (Rb_2ZnCl_4, Rb_2ZnBr_4, ...) because of the paraphase mirror plane symmetry.[10] The leading behavior is there given by the quadratic term. In high-field NMR the linear or quadratic dependence is determined by the orientation of the crystal in the magnetic field, i.e., by the relative orientation of the EFG tensor eigenframe with respect to the external magnetic field. The symmetry of the EFG tensor elements in the EFG eigenframe, which determine the V_{zz} element in the laboratory frame, determine the linear, quadratic, or mixed linear-quadratic dependence of the resonance frequency.

We calculate now the quadrupolar spin-echo attenuation in an inhomogeneous EFG in the presence of diffusion. We use the classical description of NMR with the following Bloch-like (Torrey) equation[11] for the transverse $M_+ = M_x + iM_y$ magnetization in the frame rotating with the frequency ω_0 around the z axis:

$$\frac{\partial M_+}{\partial t} = -i[\omega(x)-\omega_0]M_+ - \frac{M_+}{T_2} + D\nabla^2 M_+ . \quad (6)$$

The same equation follows from the semiclassical description of NQR.[12] The solution depends on the particular form of $\omega(x)$ and is generally different for the cases when linear or quadratic terms dominate the expansion of Eq. (5). We will first look for the exact solution of the problem.

A. Exact solution

The diffusional Bloch equation in a sinusoidal EFG can be mathematically solved exactly. We will consider separately the cases of linear and quadratic frequency-space relations.

1. Linear case

The frequency-space relation in the linear case takes the form

$$\omega(x) = \omega_0 + \omega_1 \cos(qx). \quad (7)$$

We seek the solution $M_+(x,t)$ in the form

$$M_+(x,t) = \sum_\omega M_+(x,\omega) e^{-i\omega t} \quad (8)$$

and get the equation for $M_+(x,\omega)$:

$$D\frac{\partial^2}{\partial x^2} M_+(x,\omega) + \left\{ i[\omega - \omega_1 \cos(qx)] - \frac{1}{T_2} \right\} M_+(x,\omega) = 0. \quad (9a)$$

Introducing a new variable $\phi = qx/2$, we can rewrite this equation in the form of *Mathieu's equation*:[13]

$$\frac{\partial^2}{\partial \phi^2} M_+(\phi,\omega) + (b_L - h_L^2 \cos^2\phi) M_+(\phi,\omega) = 0, \quad (9b)$$

with

$$b_L = \frac{4}{q^2 D}\left[i(\omega+\omega_1) - \frac{1}{T_2} \right] \quad (10a)$$

and

$$h_L^2 = \frac{i8\omega_1}{q^2 D}. \quad (10b)$$

Here the subscript L indicates the linear case. Mathieu's equation represents a mathematically exactly solvable problem. The solutions for the case where ϕ is a periodic variable are called *Mathieu functions* and represent infinite series of sine and cosine terms which generally do not converge. The Mathieu functions are shown in the Appendix.

2. Quadratic case

The frequency-space relation here takes the form

$$\omega(x) = \omega_0 + \omega_2 \cos^2(qx). \quad (11)$$

We again seek the solution for $M_+(x,t)$ in the form of Eq. (8). Introducing a new variable $\psi = qx$, we get the following equation for $M_+(\psi,\omega)$:

$$\frac{\partial^2}{\partial \psi^2} M_+(\psi,\omega) + (b_Q - h_Q^2 \cos^2\psi) M_+(\psi,\omega) = 0, \quad (12)$$

with

$$b_Q = \frac{1}{q^2 D}\left(i\omega - \frac{1}{T_2} \right), \quad (13a)$$

$$h_Q^2 = \frac{i\omega_2}{q^2 D}. \quad (13b)$$

This is again Mathieu's equation with the solutions in the form of Mathieu functions.

B. Solution for a short-spatial-scale diffusion

The problem of diffusion in a sinusoidal EFG is mathematically exactly solvable, but the solutions in the form of Mathieu functions do not converge and the calculation of coefficients B (see the Appendix) is also complicated. There is thus little hope that the experimental data could be properly analyzed with the exact solutions in an analytical way. A simplification of the problem can be made by considering the diffusion on a spatial scale short compared to the wavelength of the modulation wave. In the context of INC structures, this is not an oversimplification of the problem as there exists a lot of evidence that the modulation wave has restricted translational degrees of freedom and undergoes thermal fluctuations in space only on a scale short compared to its wavelength. Clear evidence is the INC broadened inhomogeneous NMR and NQR line shapes, which—except very close to T_I—show the shape of a quasistatic modulation wave.[2,9] If large-scale fluctuations exist, they are slow on the time scales of NMR spin lattice (MHz) and line shape (kHz) techniques and have not been experimentally observed so far.

For a short-scale motion we make a Taylor series expansion of the space-dependent frequency $\omega(x)$ of Eq. (5) around a certain point in space x_0 and keep the lowest-order terms only. Both problems of diffusion in a linear[7] and parabolic[14,15] potential have been solved exactly.

The frequency $\omega(x)$ is expanded in Taylor series around a general point x_0 as

$$\omega(x)=\omega(x_0)+\omega'(x-x_0)+\tfrac{1}{2}\omega''(x-x_0)^2, \quad (14)$$

where the derivatives $\omega'=(\partial\omega/\partial x)_{x_0}$ and $\omega''=(\partial^2\omega/\partial x^2)_{x_0}$ are taken at the point x_0. We find the solution of Eq. (6) for $M_+(x,t)$ in the vicinity of x_0 as[14]

$$M_+(x,t)=M_+(x,0)\exp\left\{-\left[\frac{t}{T_2}+\eta(t)\right]-i\left[\omega(x_0)t+(x-x_0)\left(\omega'+\frac{(x-x_0)\omega''}{2}\right)X(t)\right]\right\}, \quad (15)$$

with

$$\eta(t)=\frac{1}{2}\ln\{\cos[(1-i)at]\}+\frac{1}{2}\,i\,\frac{\omega'^2}{\omega''}\left\{\frac{1+i}{2a}\tan[(1-i)at]-t\right\}, \quad (16a)$$

$$X(t)=\frac{1+i}{2a}\tan[(1-i)at], \quad (16b)$$

and

$$a=\sqrt{D\omega''}. \quad (16c)$$

We can get a simple physical insight into the solutions by considering the limiting case $at<1$. This condition states that either ω'' is small or the expressions describe the short-time behavior of the transverse magnetization only when ω'' is large. In this limit we get

$$X(t)\approx t-\frac{2i}{3}D\omega''t^3, \quad (17a)$$

$$\eta(t)=\tfrac{1}{3}D\omega'^2t^3, \quad (17b)$$

yielding the following expression for $M_+(x,t)$:

$$M_+(x,t)=M_+(x,0)\exp\left\{-\frac{t}{T_2}\right\}\exp\left\{-\frac{1}{3}D\left[\omega'^2+2\omega''\times\left(\omega'(x-x_0)+\frac{1}{2}\omega''(x-x_0)^2\right)\right]t^3\right\}\times\exp\{-i\omega(x)t\}. \quad (18)$$

We find now the spin-echo attenuation in a two-pulse sequence with the pulse separation τ. At time $t=2\tau$, the phase factor refocuses and we get the echo amplitude attenuation factor $A(x,2\tau)=M_+(x,2\tau)/M_+(x,0)$ as

$$A(x,2\tau)=\exp\left\{-\frac{2\tau}{T_2}\right\}\exp\left\{-D(\nabla\omega)^2\frac{2\tau^3}{3}\right\}, \quad (19)$$

where $(\nabla\omega)^2$ represents the square effective gradient at the position x:

$$(\nabla\omega)^2=\omega'^2+2\omega''[\omega'(x-x_0)+\tfrac{1}{2}\omega''(x-x_0)^2]. \quad (20)$$

Equation (19) shows an exponential diffusive decay with the exponent proportional to the cube of time.

In the diffusion on a short scale, we can approximate the effective gradient at each point of the modulation wave by the linear term $\nabla\omega\approx\omega'$. This approximation enables us to obtain the variation of the echo attenuation at any point x of the modulation wave as

$$A(x,2\tau)=\exp\left\{-\frac{2\tau}{T_2}\right\}\exp\left\{-D\omega'^2\frac{2\tau^3}{3}\right\}. \quad (21)$$

Here the dependence on x arises from the spatial dependence of the derivative $\omega'=\omega'(x)$. Equation (21) is completely analogous to the case of a linear magnetic-field gradient [Eq. (1)]. This is not surprising as we have approximated the actual gradient of $\omega(x)$ at each point by a linear one. The exponential τ^3 decay is a consequence of this linear approximation. It is valid for arbitrary long τ as long as the diffusive motion takes place on a scale short enough that the linear approximation is reasonable. For a larger-scale motion in a nonlinear gradient, full expressions of $\eta(t)$ and $X(t)$ [Eqs. (16a) and (16b)] no longer yield the exponential τ^3 decay for long τ. The short-time part of the decay is, however, still properly described by this form as for small τ the diffusion distances are still small and the motion is effectively of a short-scale type. The deviation from the exponential τ^3 dependence at long τ's provides a way to discriminate between the short- and large-scale diffusion.

We analyze now separately the cases of linear and quadratic dependence of $\omega(x)$ on the factor $\cos(qx)$.

1. Linear case

The derivative of Eq. (7) is obtained as $\omega'(x)=-\omega_1 q\sin(qx)$. We express the factor $\sin(qx)$ using Eq. (7) as

$$\sin(qx)=\sqrt{1-\left(\frac{\omega-\omega_0}{\omega_1}\right)^2}, \quad (22)$$

so that we can convert the spatial dependence into the frequency dependence. The echo attenuation $A(\omega,2\tau)$ now becomes

$$A(\omega,2\tau)=\exp\left\{-\frac{2\tau}{T_2}\right\}\times\exp\left\{-D(\omega_1 q)^2\left[1-\left(\frac{\omega-\omega_0}{\omega_1}\right)^2\right]\frac{2\tau^3}{3}\right\}. \quad (23)$$

We consider now the variation of the diffusion-induced decay over the INC NMR spectrum. The inhomogeneous frequency distribution function $f(\omega)$, which determines the INC spectrum shape, is in the linear case obtained as[9]

$$f(\omega)=\frac{1}{\sqrt{1-[(\omega-\omega_0)/\omega_1]^2}}. \quad (24)$$

The spectrum shows two singularities at $\omega=\omega_0\pm\omega_1$ [Fig. 1(a)] and the distance between the singularities is $2\omega_1$. The intensity of the singularities comes from the nuclei, which lie close to the extrema ($qx\approx n\pi$) of the modulation wave, where the resonance frequency changes slowly. The nuclei at

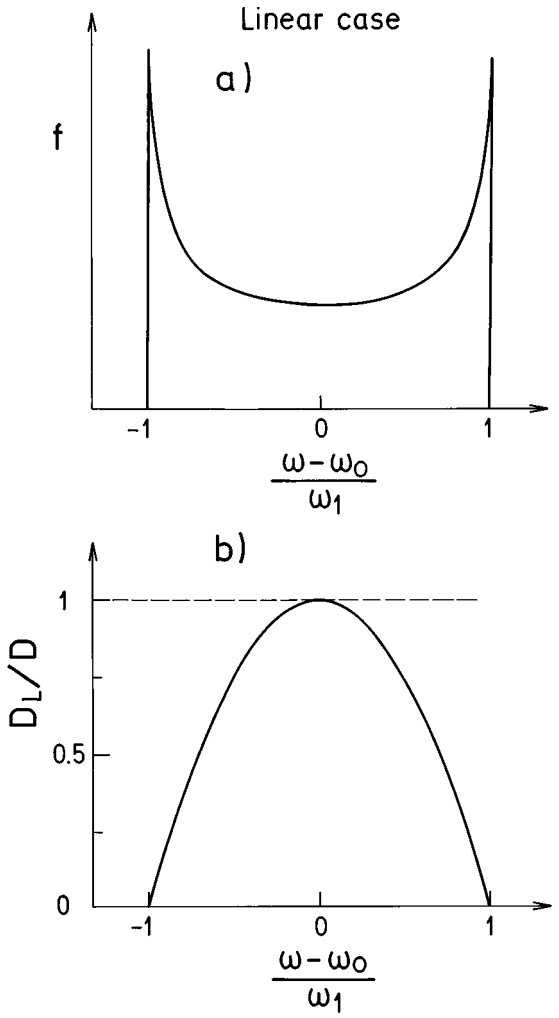

FIG. 1. (a) Inhomogeneous frequency distribution function $f(\omega)$ determining the spectrum shape in the INC phase for the linear case. (b) Variation of the frequency-dependent diffusion constant D_L over the spectrum for the linear case.

positions $qx \approx (2n+1)\pi/2$ give rise to the intensity in the middle of the spectrum, where the frequency change in space is the largest.

The diffusion-induced decay of the spectrum is frequency dependent; i.e., different parts are affected by the diffusion motion to a different extent. In Fig. 1(b) we show the frequency-dependent diffusion constant

$$D_L = D\left[1-\left(\frac{\omega-\omega_0}{\omega_1}\right)^2\right], \tag{25}$$

where the subscript L stands for the linear case. The decay is the strongest in the center of the spectrum at $\omega \approx \omega_0$ where the frequency-dependent diffusion constant equals to the true diffusion constant, $D_L = D$. Going away from the center, D_L is getting smaller, reflecting the fact that the frequency changes with space are smaller when the extrema of the sinusoidal modulation wave are approached. Exactly at the edge singularities, the diffusion-induced damping vanishes ($D_L = 0$ at $\omega = \omega_0 \pm \omega_1$) as a consequence of the fact that the gradient of the resonance frequency at the extrema is zero. A short-distance spatial motion cannot be detected at the singularities as there is no frequency change associated with that motion. The true diffusion constant D can be thus in principle obtained by measuring the spin-echo decay in the center of the spectrum. It is, however, more accurate to determine experimentally the variation of D_L over the whole spectrum and extract D from Eq. (25). To evaluate the actual D values, one needs to know the parameters ω_1 and q. The ω_1 values are obtained from the splitting of the spectrum's singularities, whereas the INC wave vector q is usually known from x-ray and neutron scattering.

2. Quadratic case

We get the derivative of Eq. (11) as $\omega'(x) = -2\omega_2 q \sin(qx)\cos(qx)$. Using Eq. (11), we convert the space dependence into the frequency dependence as

$$\sin(qx)\cos(qx) = \sqrt{\left(\frac{\omega-\omega_0}{\omega_2}\right)\left(1-\frac{\omega-\omega_0}{\omega_2}\right)} \tag{26}$$

and obtain the echo attenuation as

$$A(\omega,2\tau) = \exp\left\{-\frac{2\tau}{T_2}\right\}\exp\left\{-D(\omega_2 q)^2 4\left(\frac{\omega-\omega_0}{\omega_2}\right)\right. \times\left.\left(1-\frac{\omega-\omega_0}{\omega_2}\right)\frac{2\tau^3}{3}\right\}. \tag{27}$$

We define the frequency-dependent diffusion constant for the quadratic case as

$$D_Q = D4\left(\frac{\omega-\omega_0}{\omega_2}\right)\left(1-\frac{\omega-\omega_0}{\omega_2}\right) \tag{28}$$

and consider the variation of the diffusion-induced damping over the NMR-NQR spectrum. The frequency distribution function determining the shape of the INC spectrum in the quadratic case is given by[9]

$$f(\omega) = \frac{1}{\sqrt{[(\omega-\omega_0)/\omega_2][1-(\omega-\omega_0)/\omega_2]}}. \tag{29}$$

It exhibits two edge singularities at $\omega = \omega_0$ and $\omega = \omega_0 + \omega_2$ and splitting between the singularities equals to ω_2 [Fig. 2(a)]. The intensity of the singularities here comes from the nuclei at the positions corresponding to the extrema of the $\cos^2(qx)$ term ($qx = n\pi/2$), whereas the nuclei at $qx \approx (2n+1)\pi/4$ contribute to the intensity in the middle of the spectrum.

The true diffusion constant is again measured in the center ($\omega = \omega_0 + \omega_2/2$) of the spectrum where $D_Q = D$. The diffusion-induced damping decreases on going away from the center and vanishes at the edge singularities, $D_Q = 0$ at $\omega = \omega_0$ and $\omega = \omega_0 + \omega_2$ [Fig. 2(b)]. The reason for that is the same as in the linear case; the resonance frequency does not change there with space in a short-scale motion.

C. Large-scale diffusion: A numerical solution

We have shown for a small-scale diffusion motion in a sinusoidal EFG that simple analytical solutions can be derived for the time dependence of the spin-echo attenuation. The solutions properly describe the situation where the mo-

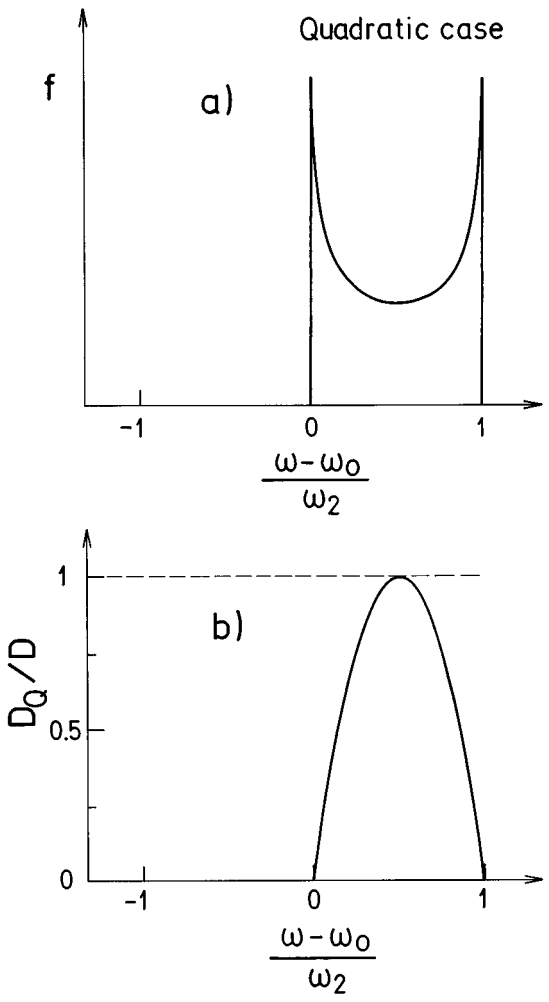

FIG. 2. (a) Inhomogeneous frequency distribution function $f(\omega)$ determining the spectrum shape in the INC phase for the quadratic case. (b) Variation of the frequency-dependent diffusion constant D_Q over the spectrum for the quadratic case.

tions extend over a space of at most few percent of the modulation wavelength. For such a motion it is permissible to approximate the actual spatial change of the resonance frequency at each point in space by a linear relation.

For a large-scale motion, no simple analytical solutions exist. A spatial motion is considered to be on a large scale when the mean diffusion length $x_{\mathrm{av}}=\sqrt{2Dt}$ in the time of experiment t is not small compared to the modulation wavelength $\lambda=2\pi/q$. In that case the diffusion-induced echo decay and the frequency dependence of the effective diffusion constant can be studied by numerical methods.

The generalized diffusion equation

$$\frac{\partial u}{\partial t}=a_0(y,t)\,\frac{\partial^2 u}{\partial y^2}+a_1(y,t)\,\frac{\partial u}{\partial y}+a_2(y,t)u \qquad (30)$$

has been numerically studied extensively.[16] Comparing this equation to Torrey's equation [Eq. (6)], we find $u=M_+$, $a_1=0$, $a_0=Dq^2$, and $y=qx$ is a renormalized space coordinate. The T_2 term has been omitted. We will find the numerical solution for the quadratic case of Eq. (11) wherefrom we get $a_2=-i\omega_2\cos^2 y$. The linear case is treated analogously ($a_2=-i\omega_1\cos y$), and the solution is qualitatively the same. The general problem of Eq. (30) is somewhat simplified as the coefficients a_n do not depend on time.

Going into the discrete space, we calculate the values of the variable u_j^n for n time steps of increment Δt and j-space steps of increment Δy using the initial condition $u_j^0=M_0$. Here M_0 is the thermal equilibrium magnetization. We find the recursion relation

$$u_j^{n+1}=u_j^n+\Delta t\left[(a_0)_j^n\,\frac{(u_{j+1}^n-2u_j^n+u_{j-1}^n)}{(\Delta y)^2}+(a_2)_j^n u_j^n\right]. \qquad (31)$$

Stable and convergent solutions are found when the condition $|a_0(y)\Delta t/(\Delta y)^2|\ll 1$ is fulfilled.[16] The calculation proceeds as follows. For every spatial point j, a set of N time values u_j^n has been calculated for the given values of D, q, and ω_2. The u_j^n values are complex due to the complex form of a_2. To mimic the complex phase factor refocusing in a spin-echo experiment, the absolute values $|u_j^n|$ were calculated. In this way numerical spin-echo attenuation curves were obtained for every spatial point.

In order to obtain the spin-echo attenuation curves at different parts of the INC spectrum, the space dependence has been converted into the frequency dependence using Eq. (11). The spectrum has been cut into 25 portions along the frequency axis, and the values of $|u_j^n|$ inside each portion have been summed up by summing over the index j. This summation has been used to mimic the determination of the spin-echo decay curves in a real experiment where the spectral intensity is integrated in small frequency intervals over the spectrum. The integration is used to get the experimental points less susceptible to the noise. The numerical decay curves were compared to the exponential t^3 decay by fitting them with an approximate formula

$$|M_+(\omega,t)|\propto\exp\left\{-D_{\mathrm{eff}}(\omega_2 q)^2\,\frac{t^3}{3}\right\}, \qquad (32)$$

where an effective diffusion constant D_{eff} has been introduced. This formula has been shown to be exact for the small-scale motion [Eq. (27)], where $D_{\mathrm{eff}}=D_Q$. It describes properly also the short-time behavior for the large-scale motion. The variation of the effective diffusion constant D_{eff} over the spectrum has been then extracted.

The values of the parameters, D, q, and ω_2 used in the numerical calculation have been taken from the ^{35}Cl NQR measurements in Rb_2ZnCl_4, shown later in the paper. The q value 2.2×10^7 cm^{-1} corresponds to a modulation wavelength of $\lambda=2.8$ nm. The spectrum width $\omega_2=2000$ Hz and the true diffusion constant value $D=5\times10^{-13}$ cm^2/s have been used. The echo attenuation curve has been calculated in time increments of $\Delta t=3\times10^{-11}$ s for 1500 points on the spectrum with a separation in space of $\Delta y=\pi/1500$. The ''accuracy'' factor $Dq^2\Delta t/(\Delta y)^2\approx10^{-3}$ was small, assuring good stability and convergence of the calculation. The variation of the effective diffusion constant D_{eff} over the spectrum is shown in Fig. 3(a). The dotted line represents the true value of D. We see that for the above choice of parameters D_{eff} shows a close resemblance to the small-scale diffusion constant D_Q [Fig. 2(b)]. The reason for that becomes clear when one calculates the mean diffusion length in the time of

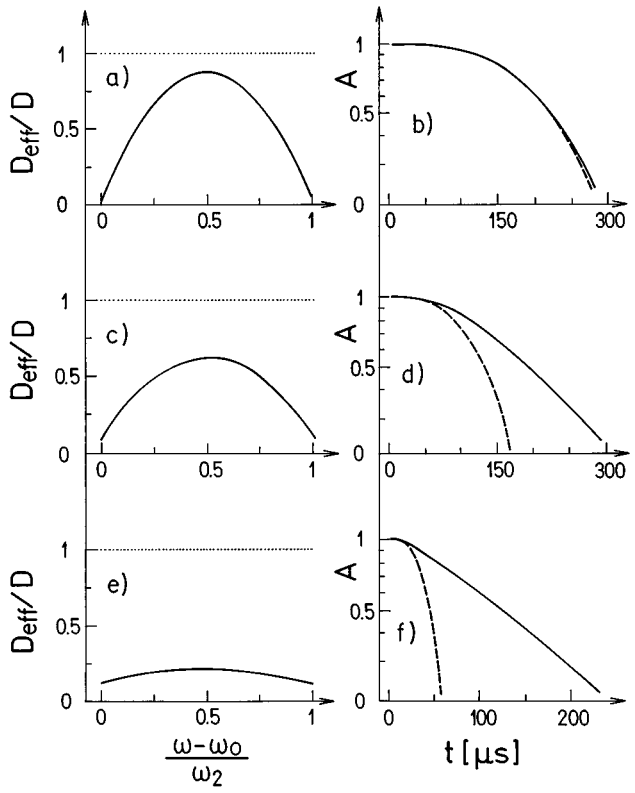

FIG. 3. Numerical solution of the diffusion equation in a sinusoidal EFG. The variation of the effective diffusion constant D_{eff} over the spectrum for the quadratic case and the spin-echo decay curves $A(t)$ are shown. The true D values are indicated by the dotted lines. The decay curves (solid lines) are taken at the position on the spectrum where D_{eff} is the largest. They are compared to the decay of the form $\exp\{-t^3\}$ (dashed lines). (a) D_{eff} for the true diffusion constant value $D=5\times10^{-13}$ cm^2/s and (b) the corresponding decay curve. For this choice of parameters, the diffusive motion is of a short-scale type and the decay is well described by the $\exp\{-t^3\}$ form. (c) D_{eff} for a 10 times larger D value ($D=5\times10^{-12}$ cm^2/s) and (d) the corresponding decay curve. The motion is no longer of a short-scale type, resulting in a deviation of the decay from the $\exp\{-t^3\}$ form. The maximum D_{eff} value is also considerably smaller than D. (e) D_{eff} for a 100 times larger D value ($D=5\times10^{-11}$ cm^2/s) and (f) the corresponding decay curve. The diffusive motion takes place now on a scale large compared to the modulation wavelength. D_{eff} shows small variation over the spectrum, and its largest value is much smaller than D. The $\exp\{-t^3\}$ fit is good only in the short-time limit, whereas the decay at longer times becomes of a $\exp\{-t\}$ type.

the experiment, which is typically 1 ms. We get $x_{\mathrm{av}}=0.31$ nm, which is small compared to $\lambda=2.8$ nm, so that we deal with a small-scale motion. The fit with Eq. (32) [Fig. 3(b)] is excellent in the whole time range as expected for small-scale motion. We notice, however, that the largest D_{eff} value, obtained in the center of the spectrum, is already smaller than the true value of D, $D_{\mathrm{eff,max}}/D=0.87$. The total variation of D_{eff} over the spectrum is $D_{\mathrm{eff,max}}/D_{\mathrm{eff,min}}=14$. The fact that $D_{\mathrm{eff,max}}$ is smaller than D can be easily understood. The contribution to the spin-echo intensity at a given frequency is coming from the nuclei, which were at the beginning of the experiment located in a space region of approximately $\pm x_{\mathrm{av}}$ around a certain point. The $D_{\mathrm{eff,max}}$ value is measured at the spatial point where the frequency gradient is the largest. In the course of experiment, the nuclei have diffused in space and reached that point in the moment when the echo is formed. During the Brownian-like random walk motion, the nuclei visited a part of space where the local gradient was smaller than that at the point, where they are spectroscopically observed. The accumulated diffusion-induced decay is thus smaller than it would be if the gradient value were constant and equal to the maximum value in the whole space, visited by the nuclei during the experiment. The experimentally determined diffusion constant thus appears smaller than the true one. This effect is small in a short-scale motion, but becomes pronounced in a large-scale motion.

In Fig. 3(c) we show the frequency dependence of D_{eff} for a 10 times larger $D=5\times10^{-12}$ cm^2/s, corresponding to $x_{\mathrm{av}}=0.99$ nm. This is now a considerable fraction of the wavelength, $x_{\mathrm{av}}/\lambda=0.35$. The maximum value of the effective diffusion constant is here considerably smaller than the true one, $D_{\mathrm{eff,max}}/D=0.62$, and the total variation is reduced, $D_{\mathrm{eff,max}}/D_{\mathrm{eff,min}}=6.1$. The fit with Eq. (32)—showing the exponential t^3 dependence—is good in the beginning (short-time) part [Fig. 3(d)]. The time dependence of the decay curve at later times becomes less strong.

For a still larger $D=5\times10^{-11}$ cm^2/s, we get $x_{\mathrm{av}}=3.15$ nm, which is already larger than the wavelength λ, $x_{\mathrm{av}}/\lambda=1.1$. Here we get [Fig. 3(e)] $D_{\mathrm{eff,max}}/D=0.21$, and the total variation $D_{\mathrm{eff,max}}/D_{\mathrm{eff,min}}=1.8$ becomes very small. The fit shows $\exp\{-t^3\}$ decay only in the short-time limit, whereas the numerical curve becomes of the $\exp\{-t\}$ type [linear on the logarithmic scale in Fig. 3(f)] at later times. We see that the large-scale motion in a sinusoidal potential averages out the variation of D_{eff} over the spectrum. The measured $D_{\mathrm{eff,max}}$ value is also much smaller than the true D value. The total variation of D_{eff} over the spectrum serves as a criterion for a discrimination between the small- and large-scale diffusion.

The above consideration of the small- and large-scale diffusion in a sinusoidal EFG applies in exactly the same way also to the diffusion in a sinusoidal magnetic-field gradient. A pronounced difference is, however, found in the size of the measured diffusion constants D. The quantity determining the range of measured D values is the magnitude of change of the resonance frequency with space. In NMR one uses linear magnetic-field gradients of typical value 100 G/cm. The frequency change per unit length is found for, e.g., ^{1}H nuclei in this gradient to be $(\gamma\,\partial H/\partial z)=2.7\times10^6$ Hz/cm or 0.27 Hz/nm on the interatomic scale. The diffusion constants in the range $D\approx10^{-5}$–10^{-8} cm^2/s can be measured in that way, where 10^{-5} cm^2/s is a typical order of magnitude found in liquids. Recently, diffusion constants of the order 10^{-11} cm^2/s have been measured in ultrahigh magnetic-field gradients of a superconducting magnet fringe field.[17]

In an inhomogeneous electric-field gradient, the variation of the resonance frequency with space is much larger, a direct consequence of the fact that the nuclear electric quadrupole interaction is orders of magnitude stronger than the magnetic Zeeman interaction. The spectrum width determining constants ω_1 and ω_2 are of the order 10^4–10^5 s^{-1}. The INC modulation wavelength is typically of the order of few nm. For example, $\omega_1=2\pi\times1$ kHz and $\lambda=2.8$ nm result in an effective gradient $\omega_1 q=1.4\times10^4$ Hz/nm, which is five orders

of magnitude larger than in the magnetic case. As a consequence, in an inhomogeneous EFG, diffusion constants many orders of magnitude smaller (such as 10^{-15} cm^2/s or even lower) can be measured than in an inhomogeneous magnetic field.

Another point to mention is that such large spatial frequency changes can be produced only by an intrinsic EFG of ionic and electronic charges. Externally applied inhomogeneous EFG's, produced, e.g., by a suitable shape of a capacitor, can not be made so large due to technical limitations. Whereas such an external inhomogeneous EFG could be made linear in principle, the shape of the internal EFG is determined by the structure and symmetry of the lattice. In modulated structures the periodicity of the inhomogeneous EFG implies that at a certain resonance frequency one is not observing ionic diffusion at a single point in space, but a diffusion of an ensemble of ions, which are distant in space for an integer periodicity length of the resonance frequency. The real space appears reduced or ''folded'' onto one such periodicity length ($\lambda/2$ in the linear or $\lambda/4$ in the quadratic case). The problem is somewhat similar to that of restricted diffusion in geometries with barriers.

In the detection of the diffusive motion via spin-echo decay, one observes the relative motion of the resonant nuclei with respect to the spatially inhomogeneous EFG. It is not possible to discriminate between the motion of a mobile nucleus in a static environment and the motion of the environment, detected by a static nucleus.

III. COMPARISON TO EXPERIMENT

The diffusionlike motion of the incommensurate modulation wave has been experimentally observed in Rb_2ZnCl_4 by ^{35}Cl NQR and in K_2SeO_4 by ^{39}K NMR.

A. ^{35}Cl NQR in Rb_2ZnCl_4

The ^{35}Cl NQR spectrum of Rb_2ZnCl_4 consists of three lines. The incommensurate effects are most clearly observed on the high-frequency line, often referred to as the Cl(1) line. In the high-temperature paraelectric phase, the Cl(1) nuclei are located on the mirror plane, whereas below $T_I=29$ °C they are displaced from that plane in a perpendicular direction and form an INC modulation wave. Since Cl(1) nuclei are located on the modulation wave, they represent the most sensitive probe to monitor the diffusive motion of the wave.

The ^{35}Cl(1) NQR frequency ν_Q is shown as a function of temperature in Fig. 4(a). Here ν_Q slowly increases when approaching T_I from above. The temperature dependence of the positions of the edge singularities in the INC phase reflects the quadratic dependence of the absorption frequency on $\cos(qx)$. Here one singularity is a continuation of the paraphase line and the splitting of the singularities is proportional to $\omega_2 \propto A^2 \propto (T_I - T)^{2\beta}$, with $\beta \approx 0.35$. The quadratic dependence is a consequence of the mirror plane symmetry[10] in the paraphase of Rb_2ZnCl_4. The temperature dependence of the parameter ω_2 is displayed in Fig. 4(b), whereas a ^{35}Cl(1) NQR spectrum in the INC phase at $T=23$ °C is shown in Fig. 4(c).

Spin-echo decay measurements were performed in the vicinity of T_I using a pulsed NQR technique. The echo envelope as a function of the interpulse spacing time τ showed, in addition to the decaying behavior, slow beats with a frequency of about 2 kHz. These oscillations could originate from the stray field of a superconducting magnet located in the vicinity of the NQR apparatus or from the indirect spin-spin interactions.[18] This effect is, however, irrelevant to our problem, it can be accounted for by the fit procedure by using a modified spin-echo attenuation factor

$$A(2\tau) = \exp\left\{-\frac{2\tau}{T_2}\right\} \exp\left\{-D_Q(\omega_2 q)^2 \frac{2\tau^3}{3}\right\} \times [1 - C \sin^2(\pi \Delta_i \tau)]. \quad (33)$$

Here C is a constant[19] of the order of 2 and Δ_i is the frequency of the slow beats.

The experimental echo decay envelopes have been determined from the spectra. At temperatures above T_I, the spectra were single peaked and the envelopes were determined at the top of the spectra. In the INC phase the envelopes were

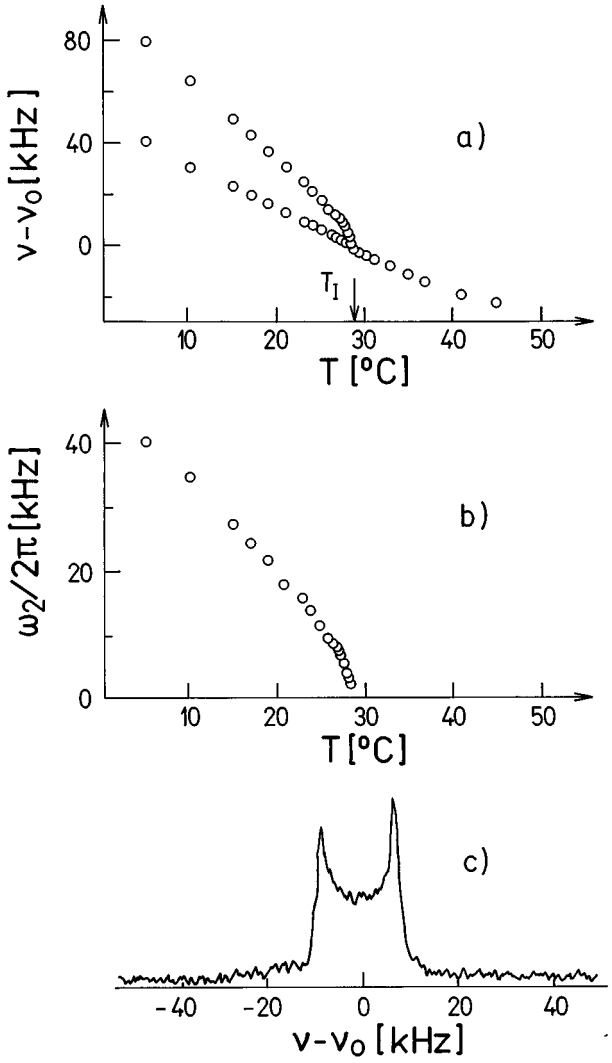

FIG. 4. (a) ^{35}Cl(1) NQR frequency ν_Q as a function of temperature in Rb_2ZnCl_4. Below $T_I=29$ °C the frequencies of the edge singularities in the spectrum are displayed. (b) Temperature dependence of the parameter ω_2 as determined from the splitting of the edge singularities. (c) ^{35}Cl(1) NQR spectrum of Rb_2ZnCl_4 in the INC phase at $T=23$ °C.

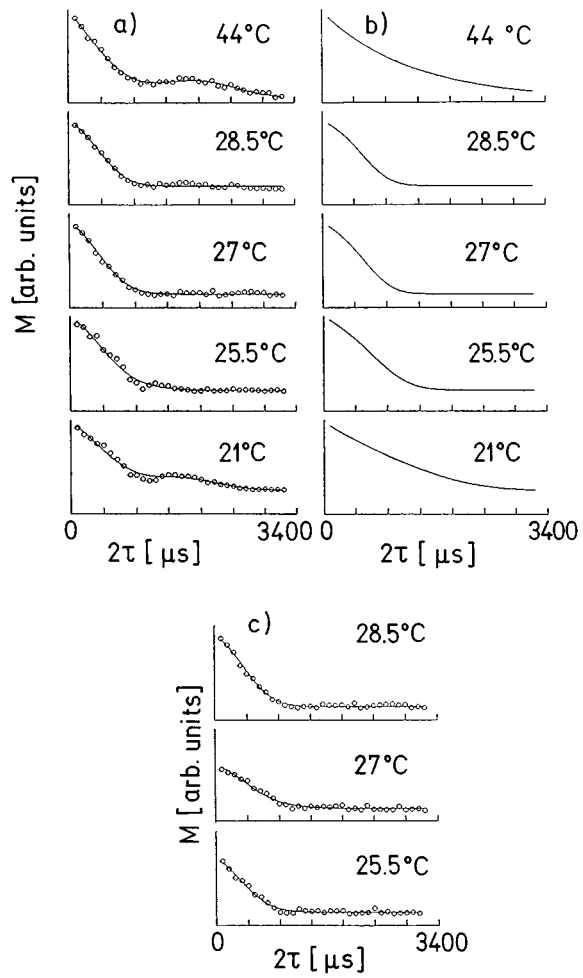

FIG. 5. (a) Temperature dependence of the ^{35}Cl(1) spin-echo decay curves in Rb_2ZnCl_4 below and above T_I. Below T_I the curves have been obtained at the high-frequency singularity of the NQR spectrum. Experimental points (circles) are shown together with the theoretical curves (solid lines), computed from Eq. (33). (b) Theoretical curves from (a) with the oscillatory part subtracted. These curves show the T_2 and diffusive decay only. The exponential decay of the form $\exp\{-2\tau/T_2\}$ far above and below T_I changes into a diffusive one of the form $\exp\{-D_Q(\omega_2 q)^2 2\tau^3/3\}$ in the vicinity of T_I. (c) Echo decay curves at the position in the middle of the spectrum.

determined selectively in small steps (typically 25) over the whole spectrum. The decay curves of the paraphase and those obtained at the high-frequency singularity of the INC spectrum are shown as a function of temperature in Fig. 5(a). Solid lines represent the fits with Eq. (33). In Fig. 5(b) only the fits are displayed with the oscillatory part subtracted. In Fig. 5(c) the curves at the position in the middle of the spectrum are shown. It is observed that far above T_I the decay is well described by the T_2 term only. This demonstrates that molecular motions of the diffusive type are not dominant there. T_2 has been determined to be 780 μs. In the vicinity of T_I a strong exponential t^3 damping is observed, indicating that the diffusive type of molecular motion is now dominant. Deep in the INC phase, the spin-echo decay is once more described by the T_2 term only, yielding the same value of T_2 as above T_I.

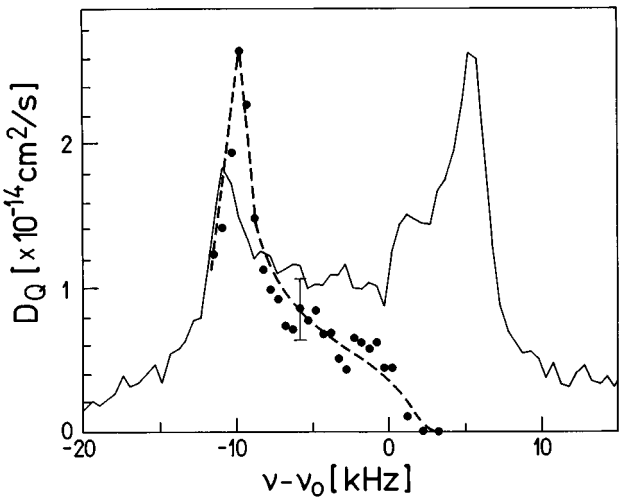

FIG. 6. Variation of the frequency-dependent diffusion constant D_Q over the ^{35}Cl(1) NQR spectrum in the INC phase of Rb_2ZnCl_4 at $T=23$ °C. The dashed line is not a theoretical fit, but serves as a guide for the eye only.

The variation of the frequency-dependent diffusion constant D_Q over the INC spectrum at $T=23$ °C is shown in Fig. 6. The values of D_Q have been extracted using the ω_2 values from Fig. 4(b) and the wave vector value[9] close to T_I $q=2.2\times10^7$ cm^{-1}. We further assumed that T_2 is constant over the region close to T_I. Here D_Q shows a pronounced variation over the spectrum. At the high-frequency singularity its value is found to be vanishingly small, $D_Q=9.8\times10^{-18}$ cm^2/s. Going towards the middle of the spectrum, D_Q increases and reaches a maximum value $D_Q=2.6\times10^{-14}$ cm^2/s close to the low-frequency singularity. Going closer to that singularity, D_Q drops again. The large total variation of D_Q over the spectrum (a factor of 2.6×10^3), the smallness of the D_Q values, and the $\exp\{-t^3\}$ shape of the spin-echo decay curves demonstrate that the diffusive motion of the INC modulation wave takes place on a scale small compared to its wavelength; i.e., it is a short-scale motion. The variation of the diffusion-induced decay over the spectrum resembles that of the pure quadratic case [Fig. 2(b)]—D_Q values are small at the singularities and reach a maximum between. The agreement is, however, only qualitative as the maximum does not appear in the middle of the spectrum, but is shifted away towards one singularity. One of the reasons for that discrepancy is the omission of the higher-order even terms in the expansion of Eq. (5). For instance, the inclusion of the $\omega_4\cos^4(qx)$ term shifts the position of the maximum frequency change in space [the condition $(\partial^2/\partial x^2)\omega(x)=0$] away from the center of the spectrum ($qx=\pi/4$) towards one edge singularity to a position determined by the solution of the equation $\cos(2qx)=-[\omega_4/(\omega_2+\omega_4)]\cos(4qx)$. The inclusion of higher-order terms increases that shift even more, and consequently the largest D_Q value is obtained somewhere between the center of the spectrum and the singularity. The second reason is a limited validity of the local approximation.[9] In a more elaborate approach, one should treat the frequency-space relation of Eq. (11) in terms of the nonlocal model.[20] The local model is strictly valid only when the wavelength of the modulation wave is large as compared

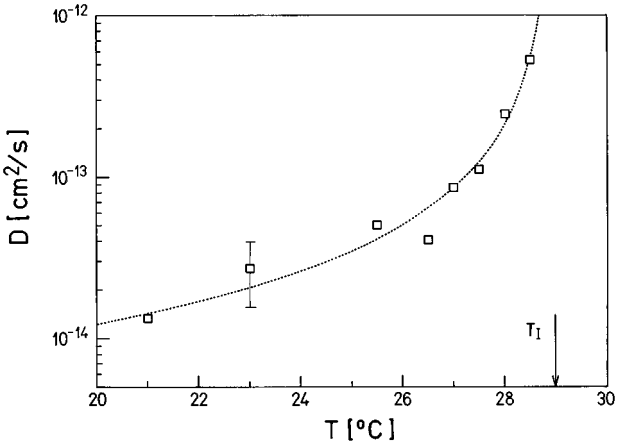

FIG. 7. Temperature dependence of the true diffusion constant D close to T_I in Rb_2ZnCl_4. Here D behaves critically in the vicinity of T_I and the fit with Eq. (34) (dotted line) yields the exponent $\lambda=1.31$.

with the radius of the region where the dominant contribution to the EFG at a given lattice site is coming from. This long-wavelength restriction is lifted in the more realistic nonlocal model.

Since the diffusive motion of the modulation wave in Rb_2ZnCl_4 is of a short-scale type, the maximum value of D_Q equals a good approximation to the true diffusion constant D. In Fig. 7, D is displayed as a function of temperature. D is the largest very close to T_I. At $T=28.5$ °C, it is equal to $D=5.3\times10^{-13}$ cm^2/s. On lowering the temperature, D drops continuously in the range 10^{-13}–10^{-14} cm^2/s. What is remarkable are the extremely low D values, which can be measured with this technique. These values are six orders of magnitude smaller than those obtained in the standard NMR pulsed magnetic-field gradient experiment and also three orders of magnitude smaller than those obtained in the fringe-field measurements. We can calculate the rms diffusion length $x_{\rm av}=\sqrt{2Dt}$ during the time of experiment which is typically 1 ms (Fig. 5). Close to T_I we find, at $T=28.5$ °C, $x_{\rm av}=0.3$ nm, which is about 10% of the INC modulation wavelength. Deeper into the INC phase, D drops to the value 1.33×10^{-14} cm^2/s at $T=21$ °C, yielding $x_{\rm av}=0.05$ nm, which is about 2% of the wavelength. This subnanometric resolution demonstrates the extreme sensitivity of this technique to the random atomic spatial motions in solids.

The temperature dependence of the diffusion constant shows that D is large in the close vicinity of T_I, whereas it diminishes rapidly on going deeper into the INC phase. This result is consistent with the previously reported thermal fluctuations of the modulation wave in Rb_2ZnCl_4 (Refs. 1 and 2), which were observed in a narrow temperature interval $\Delta T\approx0.4$ K just below T_I. Such a behavior can be explained by considering the diffusive motion of the INC modulation wave to originate from a thermal depinning of the wave at the impurity pinning centers. In the strong pinning limit,[21] the random-walk-type motion of the modulation wave can be considered as activated over a barrier[22,23] $U(A)=2WA^{\nu}$. Here we made the conjecture that $U(A)$ depends on the νth power of the amplitude $A\propto(T_I-T)^{\beta}$ of the INC modulation wave and W is a coupling constant characterizing the impurity pinning strength. Such a motion is described by a diffusion constant $D=l^2/\tau_D$, where l is the elementary step of the random walk and τ_D is the transition time per step, which is taken as thermally activated, $\tau_D=\tau_{D_0}\exp[U(A)/k_BT]$. The elementary step l is connected to the impurity density[22] $n(W)$ as $l(W)\propto n(W)^{-1/3}$, where it is considered that n depends on the impurity pinning strength W. For simplicity, we assume that $n(W)$ can be written in the form $n(W)=bW^{-\gamma}$ and calculate the average diffusion constant as

$$D=\int_0^{\infty} n(W)\,\frac{l^2(W)}{\tau_D}\,dW\propto(T_I-T)^{-\lambda}, \tag{34}$$

where $\lambda=\nu\beta(1-\gamma/3)$. According to Eq. (34), D behaves critically around T_I and rapidly decreases on lowering the temperature, as observed also experimentally. Deep inside the INC phase, diffusional effects become insignificant. Theoretical curve in Fig. 7 has been calculated with Eq. (34), and the fit yielded the exponent $\lambda=1.31$.

The present study reports to the author's knowledge the first determination of the diffusion constant by the zero-field NQR technique.

B. ^{39}K NMR in K_2SeO_4

K_2SeO_4 undergoes a transition to an INC phase at $T_I=128$ K. The ^{39}K NMR spectrum in the paraphase consists of four lines[24] at a general orientation, whereas for special orientations ($a\perp H_0$, $c\perp H_0$) this number is reduced to 2. Here we are using the same notation for the crystal axes as in Ref. 24. The experiment has been performed at the orientation $a\perp H_0$, $\angle c$, $H_0=60°$ in a 9-T magnet [$\nu_0(^{39}\mathrm{K})=17.732$ MHz]. At this orientation the frequency-space relation of Eq. (5) is linear. This is evident from Fig. 8(a) where the positions of the K(1) and K(2) lines are shown as a function of temperature. In the INC phase edge singularities of the spectra are observed symmetrically with respect to the paraphase line positions. The splitting of the singularities equals to $2\omega_1\propto A\propto(T_I-T)^{\beta}$, with $\beta\approx0.33$. In Fig. 8(b) the parameter ω_1 is displayed as a function of temperature for the K(2) line. The ^{39}K spectrum in the temperature interval 120 K$\leqslant T\leqslant$135 K is shown in Fig. 8(c).

Spin-echo decay measurements were performed from $T_I=128$ K down to 113 K. Below that temperature K(1) and K(2) lines start to overlap and a separate analysis of the diffusion effects on the two lines is no longer possible. The pulse sequence used was the usual 90-τ-180-τ-echo with the phase cycling of the 180 pulse ($\pm X$) to eliminate the relaxed magnetization. The Cyclops quadrature-error-compensating scheme has been superimposed on the phase cycle. Spin-echo decay envelopes were determined in a frequency-selective manner in small steps over the entire ^{39}K spectrum. A typical decay curve at $T=125$ K is displayed in Fig. 9. It is clearly evident that the decay is of the diffusional $\exp\{-t^3\}$ type. The solid line represents the fit with Eq. (23), whereas the dotted line shows a comparison to the pure T_2 decay, obtained by setting $D=0$ in Eq. (23). It is seen that the T_2 term only cannot reproduce the decay curve. The T_2 constant has been determined at several temperatures above and below T_I. Its values have been found in the range 56–60 ms.

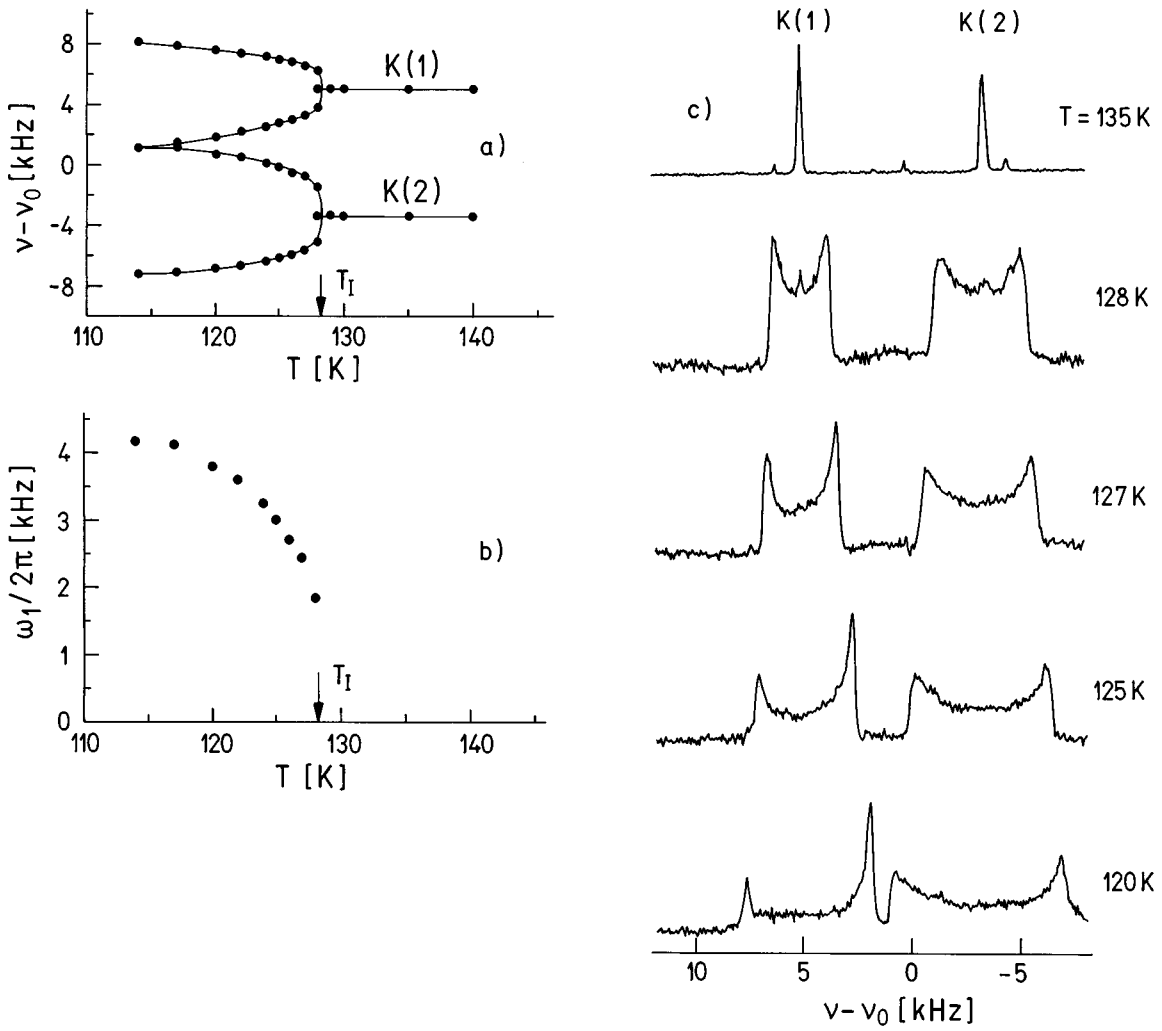

FIG. 8. (a) Temperature dependence of the ^{39}K NMR frequencies in K_2SeO_4 [$\nu_0(^{39}K)=17.732$ MHz, $a\perp H_0$, $\angle c$, $H_0=60°$]. Below $T_I=128$ K, the frequencies of the edge singularities of two physically inequivalent K(1) and K(2) lines are displayed. (b) Temperature dependence of the parameter ω_1 for the K(2) line as determined from the splitting of the edge singularities in the INC phase. (c) ^{39}K NMR spectrum at the above orientation in the temperature interval 120 K$\leqslant T\leqslant$135 K.

For the determination of the diffusion constant, we used a fixed predetermined value $T_2=58$ ms throughout the whole temperature range.

It is interesting to compare the time scales of the ^{39}K T_2 in K_2SeO_4 and the ^{35}Cl T_2 in Rb_2ZnCl_4 discussed in the previous section. T_2 imposes a limitation on the size of the diffusion constant, which can be observed in the spin-echo decay measurement. The ^{35}Cl T_2 amounts to 780 μs, whereas the ^{39}K T_2 is 58 ms. The much longer T_2 in the ^{39}K case makes it possible to trace the diffusion-induced decay longer in time so that much smaller diffusion constants already produce measurable damping effects on the echo decay curve. ^{39}K NMR measurements in K_2SeO_4 are thus more sensitive to the diffusion motion for about two orders of magnitude than those of ^{35}Cl NQR in Rb_2ZnCl_4. One of the reasons for the long ^{39}K T_2 (narrow homogeneous line width) is a small magnetic dipole moment of ^{39}K nuclei which reduces the dipolar contribution to the homogeneous broadening. The ^{39}K homogeneous linewidth in K_2SeO_4 is extremely narrow

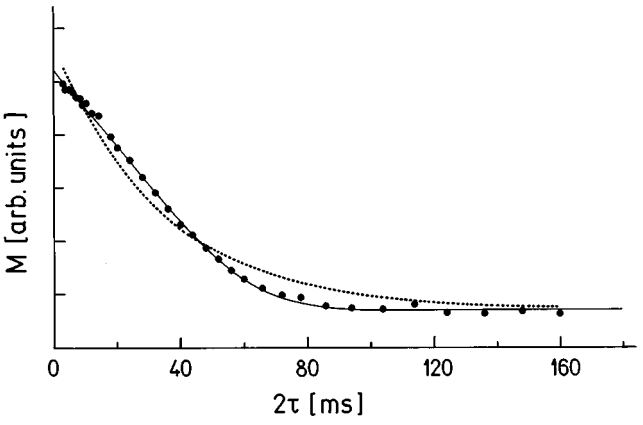

FIG. 9. ^{39}K(2) spin-echo decay curve in K_2SeO_4 at $T=125$ K obtained in the middle of the K(2) line. The solid line represents the fit with Eq. (23), characteristic for the presence of diffusion. The pure T_2 decay fit (dotted line) is shown for comparison.

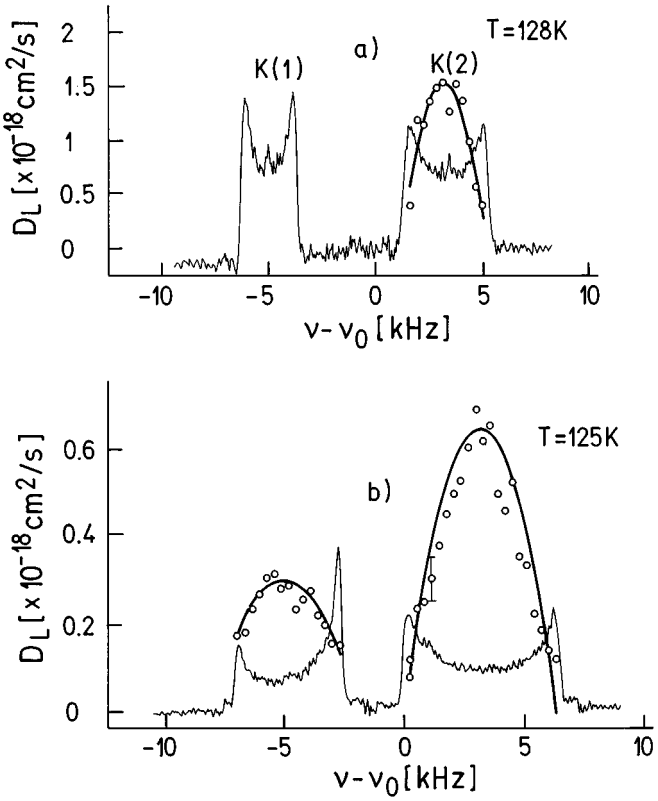

FIG. 10. Variation of the frequency-dependent diffusion constant D_L over the ^{39}K spectrum in K_2SeO_4 at $T=128$ K (a) and $T=125$ K. (b) Solid lines represent fits with Eq. (25).

[full width at half maximum (FWHM) $\Delta\nu_{1/2}=1/\pi T_2\approx 5$ Hz], whereas it is considerably broader ($\Delta\nu_{1/2}\approx 410$ Hz) in the ^{35}Cl NQR case in Rb_2ZnCl_4.

The variation of the frequency-dependent diffusion constant D_L over the spectrum is shown in Fig. 10. For the determination of D_L, the wave vector $q=(\frac{1}{3}-\delta)c^*$ $\approx 2.7\times 10^7$ cm^{-1} close to T_I has been used.[25] The agreement with the theoretical prediction of Eq. (25) (solid lines in Fig. 10) is excellent. D_L is the largest in the middle of the INC spectrum and falls off towards the singularities as predicted for a short-scale diffusion motion. For the K(2) line $D_{L,\max}$ amounts to 1.5×10^{-18} cm^2/s at $T_I=128$ K [Fig. 10(a)] and the total variation over the spectrum is $D_{L,\max}/D_{L,\min}\approx 4$. By lowering the temperature this variation increases and amounts to a factor of 7.5 [Fig. 10(b)] at $T=125$ K. Such an increase is consistent with the decrease of the true diffusion constant on going away from T_I into the INC phase, as demonstrated in Fig. 3. The true diffusion constant D has been determined from the maximum of the frequency-dependent diffusion constant D_L at each temperature. D is displayed as a function of temperature in Fig. 11. In the vicinity of T_I, D behaves critically in a similar way as in Rb_2ZnCl_4. The fit with Eq. (34) yields the exponent $\lambda=0.52\pm 0.03$. The values of D are, however, much smaller than in Rb_2ZnCl_4. One of the reasons is the fact that the INC phase occurs in K_2SeO_4 at a much lower temperature ($T_I=128$ K) than in Rb_2ZnCl_4 ($T_I=302$ K). The thermally induced motional mechanism—which requires the exchange of thermal energy with the lattice—is much less efficient at these low temperatures.

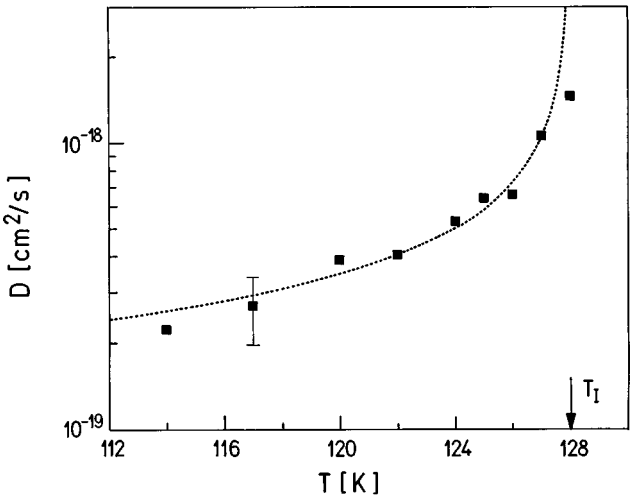

FIG. 11. Temperature dependence of the true diffusion constant D below $T_I=128$ K in K_2SeO_4. The dotted line represents the fit with Eq. (34), yielding $\lambda=0.52\pm 0.03$.

The exponential form of the spin-echo decay with the exponent proportional to the cube of time and the variation of the frequency-dependent diffusion constant over the spectrum indicate that the detected motion is of a diffusional character in a sinusoidal potential. The extremely small true diffusion constant values in the range 10^{-18} cm^2/s indicate, however, that it is no longer appropriate to speak in terms of translational diffusion of the modulation wave. What is in fact observed are slow random EFG tensor fluctuations at the ^{39}K lattice sites with sub-kHz frequencies which appear on the spatial scale comparable or smaller than the interatomic distances. These random walk fluctuations originate from both the thermal motion of the modulation wave and the thermal motion of the rest of the lattice ions which contribute to the EFG at the ^{39}K sites.

IV. CONCLUSIONS

Slow random-walk-type motion of the modulation wave in structurally incommensurate systems represents a collective atomic self-diffusion in solids. The diffusion constant D for the thermally induced modulation wave motion can be determined using a technique based on NMR and NQR in an inhomogeneous electric-field gradient which varies sinusoidally with space. The diffusion motion is detected via the changes of the quadrupole perturbed NMR or pure quadrupole NQR resonance frequencies of a nucleus which moves relatively to the spatially inhomogeneous electric-field gradient, produced by the lattice ions and electrons. The technique is capable of measuring extremely low diffusion constants such as 10^{-15} cm^2/s or even lower, so that the spatial motion is observed on the nanometric scale. The method is superior to the standard NMR technique in a pulsed-linear-magnetic-field gradient where diffusion constants smaller than 10^{-9} cm^2/s or atomic displacements smaller than 100 nm are not easily detected. Thermally induced modulation wave motion in structurally incommensurate systems, on the other hand, takes place on a much smaller scale and cannot be detected with the standard NMR technique. In the method presented

here, the resonance frequency variation with space originates from the electrostatic coupling of the nuclear electric quadrupole moments with the local electric-field gradients, which is orders of magnitude larger than the variation produced by the magnetic coupling of nuclear magnetic dipole moments with the external magnetic-field gradients. This large spatial variation makes the slow collective atomic self-diffusion in solids observable and represents currently the most sensitive method for such studies. The technique is generally applicable to the study of the modulated superstructure motions like the modulation wave motion in structurally incommensurate insulators and charge-density-wave and spin-density-wave systems as well as the motion of the vortex flux lines in type-II superconductors. It should be noted that the appearance of the exponential t^3 echo decay in a spatially inhomogeneous EFG is not restricted to the modulated structures only, but can be found rather generally in quadrupolar systems with inhomogeneously broadened absorption lines. In modulated systems, however, a well-defined resonance frequency-space relation exists, so that the intrinsic frequency gradient is known and the diffusion constant can be extracted from the spin-echo decay. This frequency gradient is not known in a general inhomogeneously broadened quadrupolar system so that D cannot be determined. Modulated structures are thus favored in this sense.

ACKNOWLEDGMENTS

The authors would like to thank to Professor Alfred Seeger from the MPI fuer Metallforschung, Stuttgart, for a stimulating discussion. The support from the NATO Scientific Affairs Division, in the framework of the Science for Stability Program and the Slovene Ministry of Science and Technology, is gratefully acknowledged.

APPENDIX

A general solution of Mathieu's equation [Eq. (9b)] can be written in the form of an infinite series:[13]

$$M_+(\phi,\omega)=e^{is\phi}\sum_{n=-\infty}^{\infty}a_n e^{2in\phi}, \tag{A1}$$

with the unknowns a_n and s. A three-term recursion formula relates the parameters a_n and s to the parameters b_L and h_L. The infinite series generally does not converge.

When the coordinate ϕ is a periodic one, returning on itself as ϕ is increased by 2π (as in our case), the solutions are also periodic and are called Mathieu functions. Four types of solutions exist: (i) even solutions of period π, $s=$even integer$=2m$,

$$[M_+(\phi,\omega)]_{e_{2m}}=\sum_{n=0}^{\infty}B_{2n}\cos(2n\phi); \tag{A2a}$$

(ii) even solutions of period 2π, $s=$odd integer$=2m+1$,

$$[M_+(\phi,\omega)]_{e_{2m+1}}=\sum_{n=0}^{\infty}B_{2n+1}\cos(2n+1)\phi; \tag{A2b}$$

(iii) odd solutions of period π, $s=$even integer$=2m$,

$$[M_+(\phi,\omega)]_{o_{2m}}=\sum_{n=1}^{\infty}B_{2n}\sin(2n\phi); \tag{A2c}$$

(iv) odd solutions of period 2π, $s=$odd integer$=2m+1$,

$$[M_+(\phi,\omega)]_{o_{2m+1}}=\sum_{n=0}^{\infty}B_{2n+1}\sin(2n+1)\phi. \tag{A2d}$$

The coefficients B depend on the values b_L, h_L, m, and n. Recursion formulas relating these quantities exist. The calculation of B's is, however, a rather lengthy calculation.

[1] A. M. Fajdiga, T. Apih, J. Dolinšek, R. Blinc, A. P. Levanyuk, S. A. Minyukov, and D. C. Ailion, Phys. Rev. Lett. **69**, 2721 (1992).
[2] J. Dolinšek, A. M. Fajdiga-Bulat, T. Apih, R. Blinc, and D. C. Ailion, Phys. Rev. B **50**, 9729 (1994).
[3] G. Papavassiliou, A. Leventis, F. Milia, and J. Dolinšek, Phys. Rev. Lett. **74**, 2387 (1995).
[4] D. C. Ailion and J. Norcross, Phys. Rev. Lett. **74**, 2383 (1995).
[5] J. H. Ross Jr., Z. Wang, and C. P. Slichter, Phys. Rev. Lett. **56**, 663 (1986).
[6] A. D. Bruce and R. A. Cowley, J. Phys. C **11**, 3609 (1978); A. D. Bruce, J. Phys. (Paris) **44**, 147 (1983).
[7] E. L. Hahn, Phys. Rev. **80**, 580 (1950).
[8] E. O. Stejskal and J. E. Tanner, J. Chem. Phys. **42**, 288 (1965).
[9] R. Blinc, P. Prelovšek, V. Rutar, J. Seliger, and S. Žumer, in *Incommensurate Phases in Dielectrics*, edited by R. Blinc and A. P. Levanyuk (North-Holland, Amsterdam, 1986), Vol. 1; R. Blinc, Phys. Rep. **79**, 331 (1981); **11**, 3609 (1978).
[10] G. Papavassiliou, A. Anagnostopoulos, and F. Milia, J. Phys. C **5**, 1 (1993).
[11] H. C. Torrey, Phys. Rev. **104**, 563 (1956).
[12] M. Bloom, E. L. Hahn, and B. Herzog, Phys. Rev. **97**, 1699 (1955).
[13] P. M. Morse and H. Feshbach, *Methods of Theoretical Physics* (McGraw-Hill, New York, 1953), Pt. I, p. 556.
[14] A. Seeger, Phys. Lett. **74A**, 259 (1979).
[15] P. LeDoussal and P. N. Sen, Phys. Rev. B **46**, 3465 (1992).
[16] R. D. Richtmyer, *Difference Methods for Initial Value Problems*, Interscience Tracts in Pure and Applied Mathematics No. 4 (Interscience, New York, 1964), p. 89.
[17] R. Kimmich, W. Unrath, G. Schnur, and E. Rommel, J. Magn. Reson. **91**, 136 (1991); F. Fujara, B. Geil, H. Sillescu, and G. Fleischer, Z. Phys. B **88**, 195 (1992).
[18] N. E. Ainbinder and J. G. Shaposhnikov, *Advances in Nuclear Quadrupole Resonance* (Heyden & Son, London, 1978), Vol. 3, p. 67.

[19] V. S. Geshishkin, N. E. Ainbinder, S. I. Gushchkin, and V. A. Shishkin, Sov. Phys. JETP **28**, 407 (1968).

[20] R. Blinc, J. Seliger, and S. Žumer, J. Phys. C **18**, 2313 (1985).

[21] R. Blinc, J. Dolinšek, P. Prelovšek, and K. Hamano, Phys. Rev. Lett. **56**, 2387 (1986).

[22] P. Prelovšek, Phase Transit. **11**, 203 (1988).

[23] R. Blinc, D. C. Ailion, J. Dolinšek, and S. Žumer, Phys. Rev. Lett. **54**, 79 (1985).

[24] B. Topič, A. von Kienlin, A. Goelzhaeuser, U. Haeberlen, and R. Blinc, Phys. Rev. B **38**, 8625 (1988).

[25] J. D. Axe, M. Iizumi, and G. Shirane, in *Incommensurate Phase in Dielectrics*, edited by R. Blinc and A. Levanyuk (North-Holland, Amsterdam, 1986), Vol. II, p. 1.